Physics in Medicine &
Biology

Characterizing an electronic–robotic targeting platform for precise and fast brain stimulation with multi-locus transcranial magnetic stimulation

IOP Publishing Phys. Med. Biol. 70 (2025) 165015 https://doi.org/10.1088/1361-6560/adf36e

Physics in Medicine & Biology

IPEM Institute of Physics and Engineering in Medicine

OPEN ACCESS

RECEIVED
9 May 2025

ACCEPTED FOR PUBLICATION
23 July 2025

PUBLISHED
13 August 2025

PAPER

Characterizing an electronic–robotic targeting platform for precise and fast brain stimulation with multi-locus transcranial magnetic stimulation

Renan H Matsuda[1,2,4,*], **Victor H Souza**[1,2,4], **Thais C Marchetti**[2], **Ana M Soto**[1], **Olli-Pekka Kahilakoski**[1], **Mikael Laine**[1], **Heikki Sinisalo**[1], **Dubravko Kicic**[1], **Pantelis Lioumis**[1,3], **Risto J Ilmoniemi**[1,5] and **Oswaldo Baffa**[2,5]

[1] Department of Neuroscience and Biomedical Engineering, Aalto University School of Science, Otakaari 3, 02150 Espoo, Finland
[2] Department of Physics, Faculty of Philosophy, Sciences and Letters of Ribeirão Preto, University of São Paulo, Av. Bandeirantes, 3900, 14040-901 Ribeirão Preto, SP, Brazil
[3] BioMag Laboratory, HUS Medical Imaging Center, Aalto University, University of Helsinki and Helsinki University Hospital, Helsinki, Finland
[4] Equal contribution in first authorship.
[5] Equal contribution in senior authorship.
[*] Author to whom any correspondence should be addressed.

E-mail: renan.matsuda@aalto.fi

Keywords: transcranial magnetic stimulation, robotized TMS, multi-locus TMS, automation, electric field

Supplementary material for this article is available online

Abstract

Background. Multi-locus TMS (mTMS) enables precise electronic control of brain stimulation targeting, eliminating the need for physical coil movement. However, with a small number of coils, the stimulation area is constrained, and manual handling of the coil array is cumbersome. Combining electronic mTMS targeting with robotics enables automated, user-independent, and precise brain stimulation protocols. *Objective*. To characterize an open-source electronic–robotic mTMS platform for rapid and accurate brain stimulation targeting. *Methods*. We developed an automated robotic mTMS positioning platform. We used a 5-coil mTMS device coupled to a collaborative robot. The stimulation targeting accuracy of the system was quantified with a TMS characterizer that measures the TMS-induced electric field (*E*-field) on a model of a spherical cortex. The induced *E*-field distortion generated by robot coupling was evaluated for each coil. We compared the repositioning accuracy of robotic–electronic system to the conventional manual positioning. *Results*. Our collaborative-robot-based system offers submillimeter precision and autonomy in positioning mTMS coil sets. The electronic–robotic mTMS platform was approximately 1.8 mm and 1.0° more accurate than the conventional manual positioning. Integrating robotics and mTMS automates brain stimulation procedures, resulting in minimal reliance on user expertise and subjective analysis. *Conclusion*. Our open-source platform combining rapid mTMS targeting with robotic precision enhances the safety and reproducibility of TMS, enabling more efficient and reliable outcomes than previous techniques.

1. Introduction

To enhance the safety and effectiveness of non-invasive brain stimulation, it is imperative to minimize user dependency by adopting automation for precise targeting of cortical structures. Multi-locus transcranial magnetic stimulation (mTMS) presents a significant advance, allowing electronic stimulation of nearby cortical regions without the need for physical movement of the stimulation coil (Nieminen *et al* 2022, Souza *et al* 2022). This technology allows interactions with local cortical networks at millisecond and millimeter scales, allowing spatially and temporally precise modulation of brain networks (Nieminen *et al* 2019, Souza *et al* 2022, Sinisalo *et al* 2023, 2025b). Traditional TMS procedures require physical movement of the coil to

target different brain areas, which can be cumbersome and limit spatiotemporal precision. mTMS has the potential to engage with brain network activities more effectively by optimizing both the spatial reach and the timing of stimulation pulses. These advances allow more precise modulation of cortical networks, which is essential for therapeutic applications requiring accurate targeting.

Despite the promising aspects of mTMS, existing coil sets encounter two primary challenges. First, mTMS has a limited electronic targeting range, in our present system a 30 mm diameter region with 5 coils, as reported previously (Nieminen *et al* 2022). Second, the coil array assembly can weigh over 16 kg for a 5-coil set with cables and connectors. Manual positioning of the coil is highly challenging due to this substantial weight, making it impractical to maintain precise placement throughout the session (Sinisalo *et al* 2023). Regular adjustments are necessary during the session to account for minor movements of the participant and the articulated arm's inherent instability, exacerbated by the coil's weight. This process can be cumbersome and can increases the study duration due to frequent repositioning. Additionally, placing such heavy weight on the participant's scalp leads to considerable discomfort and strains on the neck muscles, hindering the recording of TMS-evoked cortical potentials with electroencephalography. Consequently, manually placing the coil set on the scalp is slow and physically demanding. These limitations restrict the application of automated algorithms, confining them to single predetermined areas and demanding highly trained and physically capable personnel for manipulating the coil sets.

Collaborative robots have demonstrated the ability to ease the process of TMS coil placement, improving the reproducibility and accuracy of reaching the desired cortical target (Goetz *et al* 2019). These robots can autonomously compensate for patients' head movements. However, existing robotized TMS applications do not seamlessly integrate with mTMS algorithms and have limited velocities (around 20 cm s^{-1}) to safely adjust the stimulation target for human applications (Kantelhardt *et al* 2010). Additionally, existing commercial robotic TMS solutions rely on closed-source platforms associated with specific robotic arms, leading to potential cost constraints and implementation difficulties. These factors prevent researchers from incorporating novel algorithms as needed. Commercial systems are typically optimized for lighter, standard TMS coils, which can be mounted off-axis and positioned farther from the robot's end effector without causing significant issues. This setup helps minimize any mutual coupling between the robot and the coil. In contrast, such a configuration is not feasible for the mTMS coil set because of its greater weight. To ensure stability and remain within the robot's payload limits, the mTMS coil must be mounted directly beneath the robot flange. Offsetting it laterally would risk compromising precision and could exceed the robot's mechanical tolerances.

Recently, we developed an open-source electronic–robotic control that seamlessly integrates rapid mTMS electronic targeting with precise and autonomous robotic handling. Our system eliminates the need for manual manipulation of mTMS coil sets, significantly improving the safety and precision of the technique. The platform is readily accessible at https://github.com/biomaglab/tms-robot-control. We have also demonstrated the initial feasibility of our system, showing its ability to perform real-time head motion compensation and automate a motor mapping experiment (Matsuda *et al* 2024, Sinisalo *et al* 2025a). However, further characterization is needed to evaluate the system's impact on the spatial precision and reproducibility of the induced electric field (*E*-field). Two factors were considered that could alter the magnetic field generated by the mTMS coil set, when used together with the collaborative robot. First, materials in robotic components could distort magnetic fields due to their magnetization potential, as described by the principles of magnetism. Second, the geometric configuration of coils and robotic parts can affect the magnetic field. Thus, changes in the robotic arm position can in principle lead to changes in the cortical *E*-field. Therefore, our goal was to characterize the accuracy and precision in targeting the induced *E*-field by combining the mTMS electronic control and the automated robotic positioning. We also evaluated the distortion in the *E*-field caused by attaching mTMS coil sets to the robot flange and compared manual and robotic electronic brain targeting. This platform opens exciting possibilities for developing new brain stimulation paradigms, such as closed-loop and operator-independent protocols capable of effectively covering large cortical brain areas.

2. Material and methods

We characterized our platform utilizing the Elfin E5 collaborative robot (Han's Robot Co Ltd, China). This robot has 6 joints, a 5 kg payload capacity, an operational range of up to 80 cm, and a repeatability accuracy of ± 0.05 mm. The electronic–robotic control was developed to operate with the open-source neuronavigation system InVesalius Navigator (Souza *et al* 2018).

To ensure safe operation during coil positioning and real-time head motion compensation, the electronic–robotic control was equipped with five independent software-based safety layers and a force–torque sensor (FT 300-S, Robotiq, Canada). The safety layers included: (1) movement permission only

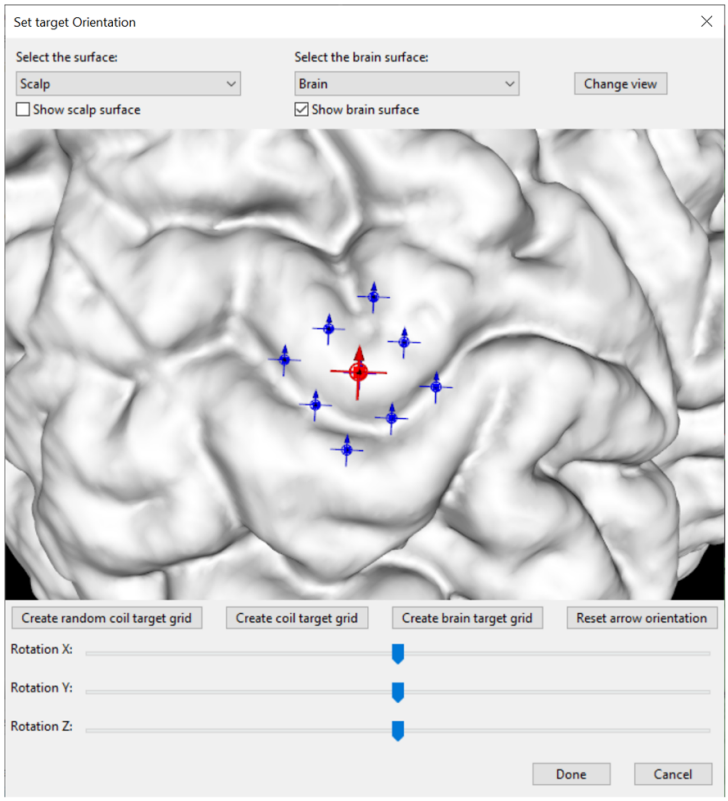

Figure 1. Graphical User Interface (GUI) for mTMS targeting. The interface allows for precise adjustments of both scalp (red arrow) and brain targets (blue arrows). The scalp target represents the physical location and orientation on the scalp where the mTMS coil set is positioned. This target is adjustable to ensure proper alignment relative to the participant's head. The brain targets indicate the cortical regions targeted for stimulation. The position and orientation of the brain targets can be adjusted manually and sent to the mTMS control software for electronic shifts within the 30 mm effective stimulation range of the mTMS coil set.

when the tracking marker on the subject's head was visible; (2) a Kalman filter to suppress sudden tracking fluctuations; (3) a head velocity estimator allowing robot motion only if head movement was below 5 mm s^{-1}; (4) spatial constraints restricting the coil's movement to a predefined safe workspace; and (5) trajectory control enforcing an arced movement path when repositioning over distances greater than 10 cm to avoid collisions. Additionally, the force–torque sensor measured contact forces in three axes and applied two safety rules: (1) if contact force exceeds 5 N, the robot immediately halts motion; and (2) if the applied force increases by more than 30% from the initial value, the robot performs a retreat motion in the opposite direction until the force drops below the 30% threshold. These features collectively ensured safe and adaptive coil positioning throughout the experiment.

We used an mTMS device with a 5-coil set and an effective stimulation range of 30 mm in diameter. The 5-coil set comprises two four-leaf-clover coils, two figure-of-eight coils, and an oval coil (Nieminen *et al* 2022).

Electronic–robotic targeting: The integration between the robotic control and the mTMS electronic targeting was implemented in InVesalius. We developed a graphical interface to define the desired brain and scalp targets for the mTMS. The scalp targets are related to the physical positioning of the mTMS coil set, establishing its location and orientation on the scalp, adjusted by the robotic arm's precise movement capabilities. The brain targets are involved in the electronic shifts of the mTMS, enabling stimulation of different cortical targets with high precision. The user can define cortical targets for the mTMS within a 30 mm diameter region around the coil set's center. These targets are projected linearly at a 15 mm depth along the coil's normal axis from the scalp target, in alignment with the spherical cortex model used for designing the 5-coil sets (Nieminen *et al* 2022), including manual control of the desired target coordinates and orientations, figure 1.

Experimental characterization: To evaluate the performance and accuracy of our open-source electronic–robotic mTMS platform, we conducted three experimental characterizations for assessing the induced *E*-field, targeting precision, and repositioning accuracy. These experiments validate the platform's capabilities by comparing the electronic targeting and robotic positioning with traditional manual methods.

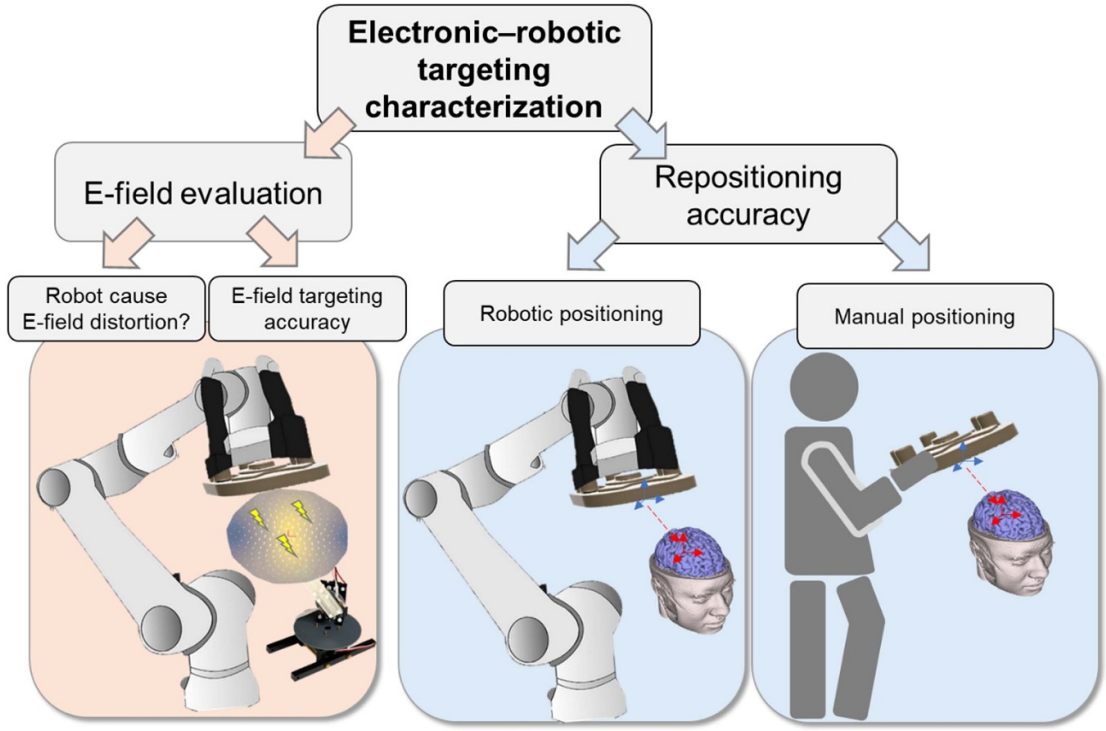

Figure 2. Workflow for experimental characterization. The flowchart shows the main steps in our experimental setup for evaluating both the accuracy and reproducibility of mTMS coil positioning, focusing on the *E*-field (light orange) and physical positioning (light blue). The *E*-field evaluation includes two steps: (1) checking whether the robot causes any *E*-field distortions and (2) measuring the accuracy of the *E*-field targeting. The leftmost illustration depicts the experimental setup, with the robotic arm and mTMS coil set positioned on top of the TMS characterizer, showing the resulting *E*-field distribution. To evaluate physical repositioning accuracy, we compare the robot-assisted and manual approaches. The middle and right illustrations show the robotic and manual positioning of the mTMS coil set. The blue axis represents the initial position, the red axis marks the scalp target, and the dashed line shows the trajectory to reach the target.

The characterization process involved three key steps: (1) evaluating potential distortions in the induced *E*-field due to the robotic setup, (2) quantifying the precision of the targeting algorithm, and (3) assessing the accuracy and repeatability of coil positioning using both robot-assisted and manual approaches. The characterization flowchart is depicted in figure 2. We measured the induced *E*-field spatial distribution on a 70 mm-radius spherical volume conductor model using our TMS characterizer (Nieminen *et al* 2015). The bottom of the mTMS coil set was placed 15 mm above the measurement probe.

(1) Evaluation of the potential distortions of the metallic components of the robot on the induced *E*-field: we verified the distortions on the *E*-field caused by attaching the mTMS coil sets to the robot flange. We measured the induced *E*-fields of each of the five mTMS coils individually, with and without the robot attached to the coil assembly. The measurement of the induced *E*-field had 250 data points in a 40 mm diameter circular area from the central point of the mTMS coil set on the spherical cortical model. We used a wooden stand below the mTMS coil set to ensure it had the same position relative to the TMS characterizer with and without the robot attached (figure 3). First, we measured with the mTMS coil set screwed to the robot flange. Then, the robotic arm was detached and moved at least 50 cm away from the measurement platform. The relative difference between the maximum *E*-field peak with and without the robot was estimated using equation (1) for each of the 5 coils.

$$\text{Relative Difference}\,(\%) = \frac{|\text{MAX\_EField}_{\text{without robot}} - \text{MAX\_EField}_{\text{with robot}}|}{\text{MAX\_EField}_{\text{without robot}}} \times 100 \qquad (1)$$

(2) Evaluation of the targeting algorithm: we characterized the robotic–electronic targeting accuracy by physically moving the coil set and compensating for this displacement with the electronic targeting algorithm. We created 10 mTMS scalp targets, which were aligned perpendicular to the TMS characterizer frame. For these targets, the roll and pitch remained constant, and only the yaw rotation was varied, selecting angles within the range of $-30°$–$30°$ relative to one of the search coils of the TMS characterizer. Scalp target locations and rotations were pseudo-randomly sampled from a uniform distribution, figure 4(a). For tracking the coil set, we used a motion capture system with eight Flex13 cameras (OptiTrack, NaturalPoint,

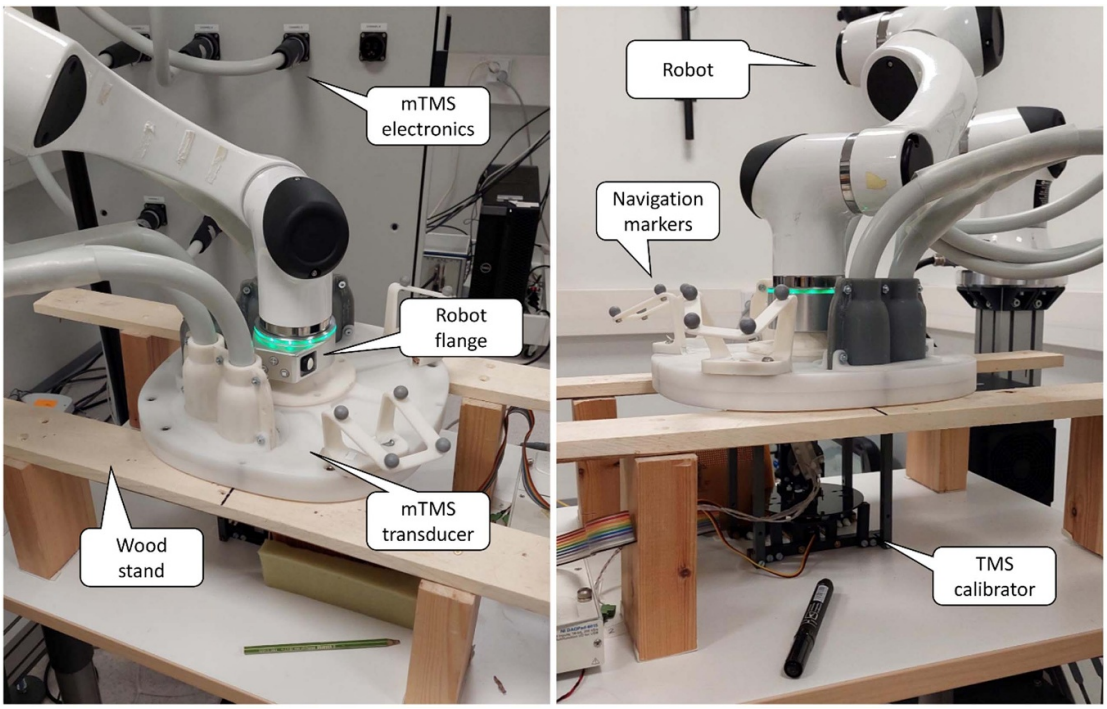

Figure 3. Experimental setup with the mTMS coil set on top of the *E*-field characterizer. Two views from the experimental setup with the mTMS coil set held by the robot on top of the TMS characterizer. The mTMS coil set is attached to the robot flange, ensuring stable positioning during measurements. Navigation markers are affixed to the coil, serving dual purposes: for neuronavigation with optical tracking and controlling the robotic arm's movements. The 5-coil set is placed on a wooden stand without any metallic components, allowing the coil set to remain in the desired position relative to the probe when the robot attachment is removed.

Inc., USA) with the InVesalius neuronavigation system (Souza *et al* 2018). Neuronavigation was performed with a magnetic resonance image (MRI) phantom with similar dimensions ($11 \times 15 \times 17$ cm^3) to the TMS characterizer. The MRI phantom comprises a set of 180 images generated in MATLAB 2022a (The MathWorks Inc, USA). The image represents a conventional 3D T1-weighted structural MRI with $256 \times 256 \times 180$ voxels of size $1 \times 1 \times 1$ mm^3, figure 4(b). The neuronavigation fiducials were defined at the bottom right and left and at the anterior top-middle of both phantom MRI and TMS characterizer, figures 4(c) and (d).

The robotized mTMS platform automatically estimates an approximate linear offset to translate the maximum *E*-field from the center of the mTMS coil set to the center of the TMS characterizer for all scalp targets. The *E*-field for each target was measured at 100 points, covering a 30 mm diameter area centered on the TMS coil. The experiment was repeated three times, resulting in 30 pseudo-random scalp targets. The centroid of the focal *E*-field area (defined as the region where the *E*-field reaches at least 70% of its peak value (Nieminen *et al* 2015)) is calculated as the weighted center of mass of the *x* and *y* coordinates, using the *E*-field magnitude as the weight, equation (2). The dispersion (standard deviation, *SD*) was computed from the *x* and *y* centroid coordinates of the focal *E*-field area, equation (3),

$$\bar{x} = \frac{\sum_{i\in\mathcal{F}} x_i E_i}{\sum_{i\in\mathcal{F}} E_i}; \quad \bar{y} = \frac{\sum_{i\in\mathcal{F}} y_i E_i}{\sum_{i\in\mathcal{F}} E_i} \tag{2}$$

where the centroid is computed in the focal area within $\mathcal{F} = \{i \,|\, E_i \geqslant \lambda E_{\max}\}$, and $\lambda E_{\max} \approx 70\%$ of the peak *E*-field.

$$\mathrm{SD}_x = \sqrt{\frac{1}{N}\sum_{j=1}^{N}\left(\overline{x_j} - \overline{x_{\mathrm{mean}}}\right)^2}; \quad \mathrm{SD}_y = \sqrt{\frac{1}{N}\sum_{j=1}^{N}\left(\overline{y_j} - \overline{y_{\mathrm{mean}}}\right)^2} \tag{3}$$

where $N = 30$ is the total number of targets and $\overline{x_j}$, $\overline{y_j}$ are the centroid coordinates for each target *j*.

(3) Comparison robotic and manual repositioning: we evaluated the accuracy of repositioning the mTMS coil set over the scalp target in two mockup experiments: firstly, with the mTMS coil set positioned by the robot and secondly, manually. We defined a scalp target approximately above the motor cortex and in an

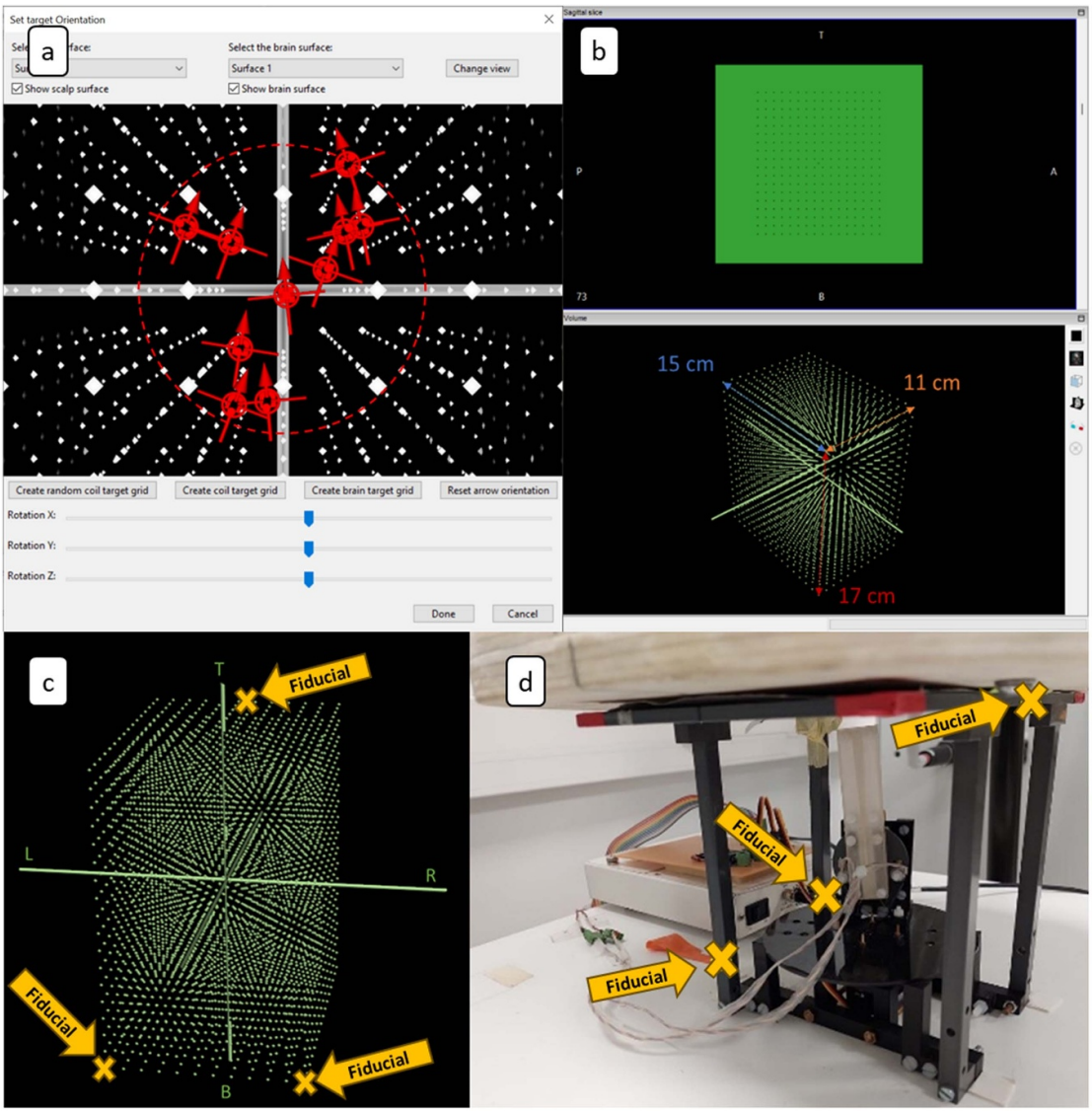

Figure 4. (a) GUI for mTMS targeting. Ten mTMS scalp targets (red arrows) were pseudo-randomly generated within a 30 mm radius (red dashed circle), with yaw rotations ranging from -30° to 30°. (b) InVesalius interface with the MRI phantom with similar dimensions as the TMS characterizer. The green dots in the 3D panel are spaced by 1 cm in all axes. (c) The MRI phantom highlights the fiducials located at the bottom right and left and at the anterior top-middle of the MRI. (d) Photograph of the TMS characterizer with fiducials placed according to the MRI.

initial arbitrary location far from a dummy head. We alternated the robot position 15 times between the target and the initial position, and repeated the same procedure for the manual positioning. The accuracy of repositioning the mTMS coil set was defined as the Euclidean distance between the predefined scalp target location and the corresponding measured final positions and orientation after each placement. We used InVesalius connected to the tracking device Polaris Vega VT (Northern Digital Inc., Canada), to record the coil coordinates. Neuronavigation was performed with the Montreal Neurological Institute average MRI (Evans *et al* 1993) based on 152 MRIs. To assess the difference in robotic and manual repositioning accuracy, we used a two-way ANOVA followed by Tukey HSD post-hoc multiple comparisons. Statistical analysis was performed with custom scripts written in R 4.2 (R Core Team, Austria). The significance threshold was set at 0.05.

3. Results

***E*-field distortion**: The robot attached to the mTMS coil set did not cause any observable differences in the *E*-field spatial distribution of all coils. The maximum *E*-field recorded with the robot attached had an average marginal increase of 3.3% $\pm$ 3.2% compared to without the robot. This increase does not substantially alter the overall spatial distribution, indicating that the presence of the robotic components did not significantly affect the spatial precision or intensity of the induced *E*-field. Figure 5 depicts the *E*-field spatial distribution

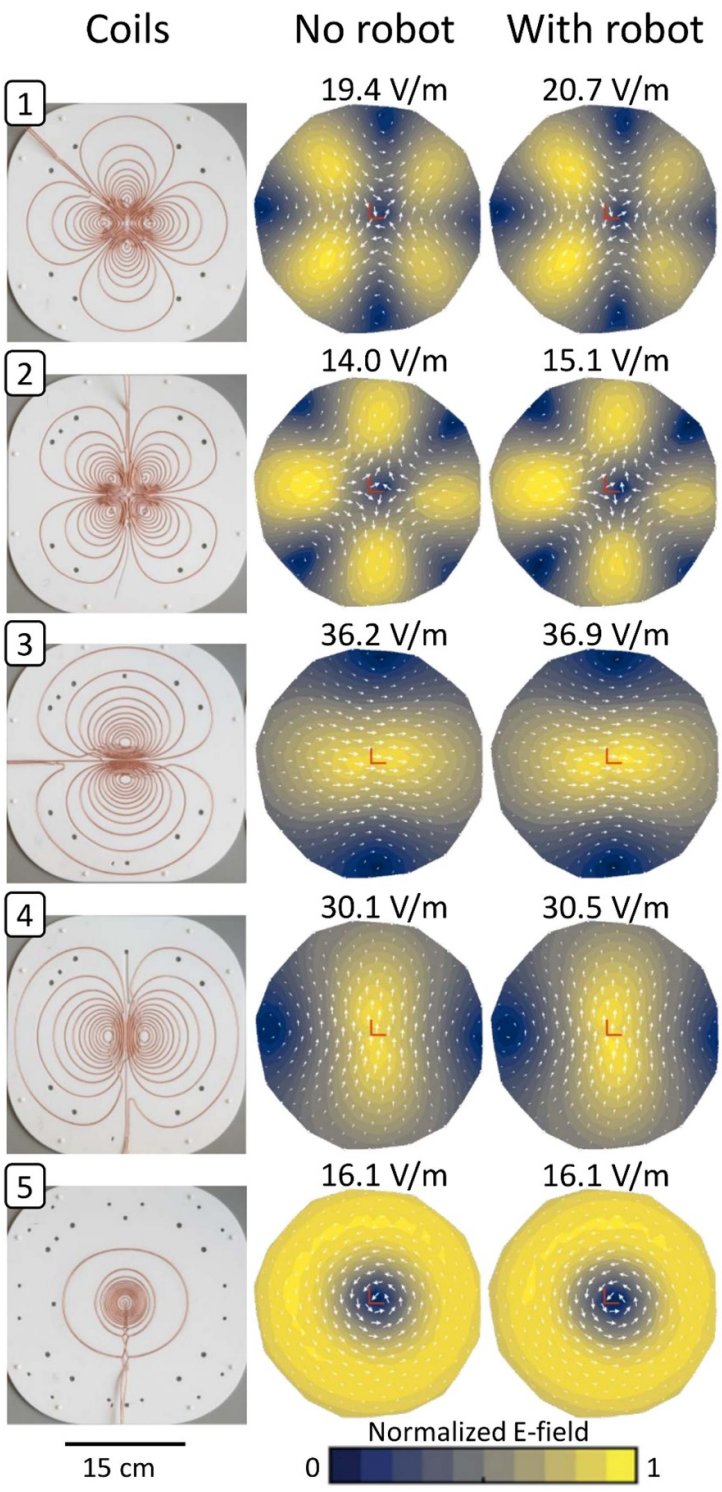

Figure 5. The 5-coil windings and their corresponding *E*-field distribution with and without the robot. The values on each *E*-field distribution represent the maximum *E*-field intensity. The red axis represents the center of the *E*-field distribution, and the *E*-field is normalized for each coil.

from the five mTMS coils, visually confirming the minimal impact of robotic attachment on field characteristics. Supplementary materials section provides a theoretical estimation of the positional offset required to explain the observed increase in field strength, yielding an estimated offset of approximately 0.18 mm.

Robotic–electronic cortical targeting accuracy: The induced *E*-field centroid dispersion of the autonomous robotized mTMS in the *x* and *y* axes were ±0.7 and ±0.2 mm, respectively. The dispersion of the peak *E*-field intensity was ±1.0 V m^{-1}. The average *E*-field distribution across all measurements is illustrated in figure 6(a).

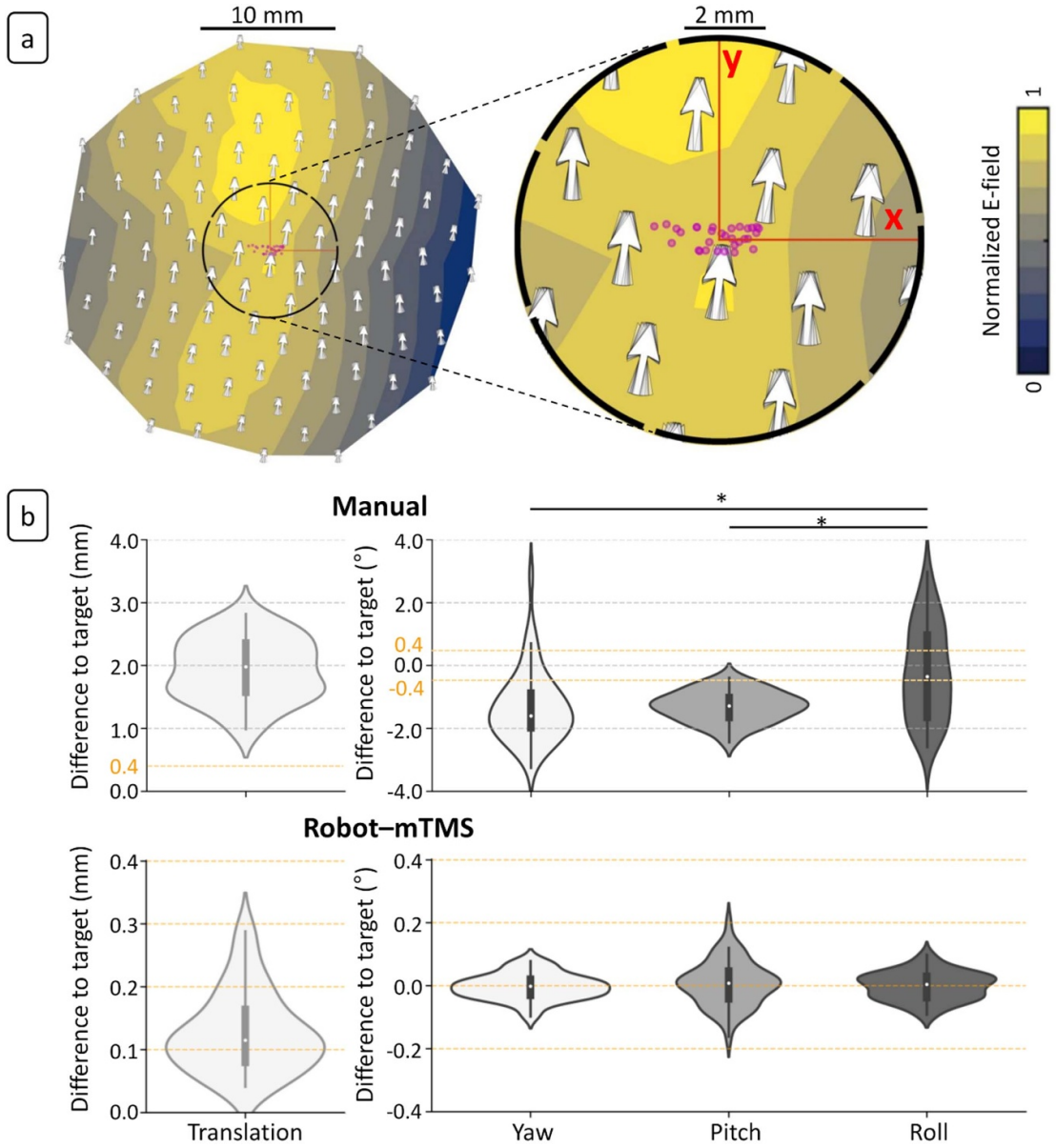

Figure 6. Experimental characterization and demonstration of robotic–electronic mTMS. (a) *E*-field dispersion of the robotized mTMS. The purple circles are the centroids of the *E*-field distributions for each mTMS target. The red axes indicate the center of the TMS characterizer, and the white arrows show the *E*-field orientation at a given characterizer's probe position. The arrows overlap over each mTMS target. The black dashed circle (10 mm diameter) indicates the spatial extent of the zoomed panel on the right side. (b) Measured accuracy in repositioning the mTMS coil set on the target manually (top panel) and with the robotic control (bottom panel). * $p < 0.001$.

Comparison of manual and robotic–electronic cortical target positioning: The average robotized positioning was about 1.8 mm and 1.0° more accurate than the manual positioning for the translation ($F_{1,95} = 646.6$; $p < 0.001$) and rotation angles ($F_{1,289} = 87.57$; $p < 0.001$), respectively. The average distance to the target with the robotized repositioning was 0.3 mm, and with orientations within −0.2°–0.2°. No difference was found between the rotation angles ($F_{2,141} = 646.6$; $p = 0.638$). The accuracy for manual repositioning was about 3.0 mm and ±3.0°. There was a significant difference within the rotation angles ($F_{2,144} = 16.52$; $p < 0.001$). The roll was 1.1° higher than the pitch ($p < 0.001$) and 1.1° smaller than the yaw ($p < 0.001$) (figure 6(b)).

4. Discussion

We leveraged the high accuracy and autonomous capabilities of a collaborative robot to enable hands-free and precise positioning of a 5-coil mTMS system. We demonstrated that attaching the mTMS coil set to the

robot flange does not alter the *E*-field spatial distribution because, if the robot coupling had affected the *E*-field due to mutual inductance, the *E*-field would have been decreased and/or deformed. Interestingly, the maximum *E*-fields are slightly higher or equal to the robot coupling than without the coupling. These increases may be caused by the robot weight applied in the wood stand that can press the coil set slightly closer to the TMS characterizer; even a small variation will cause an observable increase in the maximum resulting *E*-fields.

Our findings have shown that the robotized–electronic system achieves superior accuracy compared to manual positioning and demonstrates comparable stability and accuracy to existing robotized TMS systems (Richter *et al* 2010, Pennimpede *et al* 2013, Grab *et al* 2018, Goetz *et al* 2019, Noccaro *et al* 2021). Although both manual and robotic coil positioning can achieve similar targeting accuracy within a predefined tolerance (e.g. 3 mm) using neuronavigation systems, the robotic system has the advantage of continuously optimizing its position to minimize spatial error beyond the threshold. This capability becomes especially valuable when working with large and heavy mTMS coils, which pose practical challenges for manual placement due to their bulkiness. While the tolerance could theoretically be reduced (e.g. to 1 mm) to improve spatial precision, achieving such precision threshold manually can be difficult and time-consuming, and may not be feasible in many clinical or research settings. In contrast, robotic systems are not limited by operator fatigue or physical constraints and can reliably maintain high spatial precision even with more stringent tolerances, suggesting a potential benefit for applications requiring highly focal stimulation or repeatable (Kantelhardt *et al* 2010, Grab *et al* 2018). While the nominal difference in positioning accuracy between manual and robotic methods is within the typical error range of TMS neuronavigation systems, the robotic system offers advantages regarding safety, stability, and long-term consistency. To ensure safe operation, we implemented a multi-layered software control strategy, including constraints on visibility, head motion velocity, spatial boundaries, and trajectory planning. Together, these features contribute to a safer and more reliable stimulation session, particularly when precise, stable, and repeatable coil placement is required over extended periods or with heavier coils like those used in mTMS (Matsuda *et al* 2024, Sinisalo *et al* 2025b). Our open-source platform for robotic–electronic targeting can be used to automate TMS protocols, including stimulation target, hotspot identification, and precise motor mapping, employing closed-loop algorithms while minimizing reliance on user experience and subjective analysis (Harquel *et al* 2017, Tervo *et al* 2020, Numssen *et al* 2021, Weise *et al* 2023).

A limitation of our robot control implementation is that the transformation between the robot and the tracking device is based on the physical location of the robot base and the tracking cameras. Thus, displacements of any of these two components will nullify the transformation matrix, compromising the robot control accuracy. A multi-camera motion capture system, such as the one used in this study, alleviates this limitation with a fixed installation. Compared to compact 2-camera models, this setup has a larger coverage volume that is less affected by the occlusion of a single camera's field-of-view and might provide more stable tracking when moving the coil set to opposing sides of the scalp, for instance, from occipital to anterior lobes. Additionally, head marker displacements cause shifts in the placement of the robotic control, leading to inaccuracies in brain stimulation. To overcome this limitation in the future, markerless head pose estimation software can be utilized (Matsuda *et al* 2023). This would add more freedom to the subjects and create a more natural experimental situation.

5. Conclusion

The development of our open-source platform, integrating electronic mTMS targeting and robotics significantly enhances the safety and reproducibility of brain stimulation procedures. We foresee that implementing automated and fast stimulation protocols fosters the creation of streamlined, user-independent, and highly efficient TMS procedures in clinical and research settings. This capability will improve treatments and allow for more sophisticated stimulation protocols to better understand cerebral functions.

Data availability statement

The data that support the findings of this study are openly available at the following URL/DOI: https://doi.org/10.5281/zenodo.15398706.

Acknowledgment

We thank Lourenço Rocha, Carlos Renato Silva, and Fernando Henrique Torrieri for technical support and the Aalto University Science-IT project for providing computational resources. This work has received funding from the Conselho Nacional de Desenvolvimento Científico e Tecnológico (CNPq) (Grant No. 141056/2018-5, 305827/2023-5), the Research Council of Finland (decisions No. 307963 and 349985), from the European Research Council (ERC) under the European Union's Horizon 2020 research and innovation programme (Grant Agreement No. 810377, ConnectToBrain), Novo Nordisk Foundation (Grant No. NNF22OC0080883 "Network Therapy with Transcranial Magnetic Stimulation", a Distinguished Innovator Grant 2-2022), and Tandem Industry Academia (decision No. 366). This article was produced as part of the activities of the FAPESP Research, Innovation and Dissemination Center for Neuromathematics (Grant Nos. 2013/07699-0, 2022/14526-3, and 2022/15500-8).

Conflict of interest

V.H.S. and O.B. are listed as inventors in a patent application for neuronavigation technology that is relevant to the methodology employed in this work. Additionally, R.J.I., H.S., and V.H.S. are inventors of patents and patent applications for TMS technologies.

ORCID iDs

Renan H Matsuda 0000-0002-1927-4824
Victor H Souza 0000-0002-0254-4322
Thais C Marchetti 0000-0002-2061-0805
Ana M Soto 0000-0002-6807-9144
Olli-Pekka Kahilakoski 0000-0003-4443-2182
Mikael Laine 0009-0003-5534-9170
Heikki Sinisalo 0009-0000-0037-8378
Dubravko Kicic 0000-0002-0576-1496
Pantelis Lioumis 0000-0003-2016-9199
Risto J Ilmoniemi 0000-0002-3340-2618
Oswaldo Baffa 0000-0002-0622-2814

References

Evans A C, Collins D L, Mills S R, Brown E D, Kelly R L and Peters T M 1993 3D statistical neuroanatomical models from 305 MRI volumes *1993 IEEE Conf. Record Nuclear Science Symp. and Medical Imaging Conf.* pp 1813–7

Goetz S M, Kozyrkov I C, Luber B, Lisanby S H, Murphy D L K, Grill W M and Peterchev A V 2019 Accuracy of robotic coil positioning during transcranial magnetic stimulation *J. Neural Eng.* **16** 054003

Grab J G, Zewdie E, Carlson H L, Kuo H-C, Ciechanski P, Hodge J, Giuffre A and Kirton A 2018 Robotic TMS mapping of motor cortex in the developing brain *J. Neurosci. Methods* **309** 41–54

Harquel S, Diard J, Raffin E, Passera B, Dall'Igna G, Marendaz C, David O and Chauvin A 2017 Automatized set-up procedure for transcranial magnetic stimulation protocols *Neuroimage* **153** 307–18

Kantelhardt S R *et al* 2010 Robot-assisted image-guided transcranial magnetic stimulation for somatotopic mapping of the motor cortex: a clinical pilot study *Acta Neurochir.* **152** 333–43

Matsuda R H, Souza V H, Kirsten P N, Ilmoniemi R J and Baffa O 2023 MarLe: markerless estimation of head pose for navigated transcranial magnetic stimulation *Phys. Eng. Sci. Med.* **46** 887–96

Matsuda R H *et al* 2024 Robotic–electronic platform for autonomous and accurate transcranial magnetic stimulation targeting *Brain Stimul.* **17** 469–72

Nieminen J O, Koponen L M and Ilmoniemi R J 2015 Experimental characterization of the electric field distribution induced by TMS devices *Brain Stimul.* **8** 582–9

Nieminen J O, Koponen L M, Mäkelä N, Souza V H, Stenroos M and Ilmoniemi R J 2019 Short-interval intracortical inhibition in human primary motor cortex: a multi-locus transcranial magnetic stimulation study *Neuroimage* **203** 116194

Nieminen J O *et al* 2022 Multi-locus transcranial magnetic stimulation system for electronically targeted brain stimulation *Brain Stimul.* **15** 116–24

Noccaro A, Mioli A, Pinardi M, Di Pino G and Formica D 2021 Development and validation of a novel calibration methodology and control approach for robot-aided transcranial magnetic stimulation (TMS) *IEEE Trans. Biomed. Eng.* **68** 1–12

Numssen O, Zier A-L, Thielscher A, Hartwigsen G, Knösche T R and Weise K 2021 Efficient high-resolution TMS mapping of the human motor cortex by nonlinear regression *Neuroimage* **245** 118654

Pennimpede G, Spedaliere L, Formica D, Di Pino G, Zollo L, Pellegrino G, Di Lazzaro V and Guglielmelli E 2013 Hot spot hound: a novel robot-assisted platform for enhancing TMS performance *Proc. Annual Int. Conf. of the IEEE Engineering in Medicine and Biology Society, EMBS* pp 6301–4

Richter L, Matthäus L, Schlaefer A and Schweikard A 2010 Fast robotic compensation of spontaneous head motion during transcranial magnetic stimulation (TMS) *UKACC Int. Conf. on CONTROL 2010. Institution of Engineering and Technology* pp 872–7

Sinisalo H et al 2025a Design, construction, and deployment of a multi-locus transcranial magnetic stimulation system for clinical use *BioMed. Eng. OnLine* **24** 61
Sinisalo H et al 2025b Multi-locus transcranial magnetic stimulation with pulse-width modulation *Brain Stimul.* **18** 948–56
Sinisalo H et al 2023 Modulating brain networks in space and time: multi-locus transcranial magnetic stimulation *Clin. Neurophysiol.* **158** 218–24
Souza V H, Matsuda R H, Peres A S C, Amorim P H J, Moraes T F, Silva J V L and Baffa O 2018 Development and characterization of the InVesalius Navigator software for navigated transcranial magnetic stimulation *J. Neurosci. Methods* **309** 109–20
Souza V H, Nieminen J O, Tugin S, Koponen L M, Baffa O and Ilmoniemi R J 2022 TMS with fast and accurate electronic control: measuring the orientation sensitivity of corticomotor pathways *Brain Stimul.* **15** 306–15
Tervo A E, Metsomaa J, Nieminen J O, Sarvas J and Ilmoniemi R J 2020 Automated search of stimulation targets with closed-loop transcranial magnetic stimulation *Neuroimage* **220** 117082
Weise K, Numssen O, Kalloch B, Zier A L, Thielscher A, Haueisen J, Hartwigsen G and Knösche T R 2023 Precise motor mapping with transcranial magnetic stimulation *Nat. Protocols* **18** 293–318